Metals **2015**, *5*, 1566-1579; doi:10.3390/met5031566

OPEN ACCESS

metals

ISSN 2075-4701

www.mdpi.com/journal/metals/

Article

Chalcopyrite Dissolution at 650 mV and 750 mV in the Presence of Pyrite

Yubiao Li [1,2,*], Gujie Qian [2], Jun Li [2] and Andrea R. Gerson [2,3,*]

[1] School of Resources and Environmental Engineering, Wuhan University of Technology, Wuhan 430070, Hubei, China

[2] Minerals and Materials Science & Technology, Mawson Institute, University of South Australia, Mawson Lakes, SA 5095, Australia; E-Mails: gujie.qian@unisa.edu.au (G.Q.); jun.li@unisa.edu.au (J.L.)

[3] Blue Minerals Consultancy, 13 Mill Terrace, Middleton, SA 5213, Australia

***** Authors to whom correspondence should be addressed; E-Mails: yubiao.li@whut.edu.cn (Y.L.); andrea.gerson@bigpond.com (A.R.G.); Tel.: +86-18702778563 (Y.L.); +61-4-22112516 (A.R.G.); Fax: +86-27-87882128 (Y.L.); +61-8-83025545 (A.R.G.).

Academic Editor: Suresh Bhargava

Received: 6 August 2015 / Accepted: 25 August 2015 / Published: 28 August 2015

Abstract: The dissolution of chalcopyrite in association with pyrite in mine waste results in the severe environmental issue of acid and metalliferous drainage (AMD). To better understand chalcopyrite dissolution, and the impact of chalcopyrite's galvanic interaction with pyrite, chalcopyrite dissolution has been examined at 75 ℃, pH 1.0, in the presence of quartz (as an inert mineral) and pyrite. The presence of pyrite increased the chalcopyrite dissolution rate by more than five times at E_h of 650 mV (SHE) (Cu recovery 2.5 *cf.* 12% over 132 days) due to galvanic interaction between chalcopyrite and pyrite. Dissolution of Cu and Fe was stoichiometric and no pyrite dissolved. Although the chalcopyrite dissolution rate at 750 mV (SHE) was approximately four-fold greater (Cu recovery of 45% within 132 days) as compared to at 650 mV in the presence of pyrite, the galvanic interaction between chalcopyrite and pyrite was negligible. Approximately all of the sulfur from the leached chalcopyrite was converted to S^0 at 750 mV, regardless of the presence of pyrite. At this E_h approximately 60% of the sulfur associated with pyrite dissolution was oxidised to S^0 and the remaining 40% was released in soluble forms, e.g., SO_4^{2-}.

Keywords: chalcopyrite; pyrite; galvanic interaction; dissolution

1. Introduction

Chalcopyrite ($CuFeS_2$) is the most abundant copper containing mineral on the planet, accounting for approximately 70% of the total copper resources [1]. Although copper is predominantly extracted using pyrometallurgical processing, much attention has recently been paid to the development of an effective hydrometallurgical extraction methodology [2–8] due to the potential for improved economics and reduced environmental impact, especially for ore of low copper grade.

The most common reaction (Equation (1)) used to describe [4,6,9–11] chalcopyrite dissolution is its oxidation by Fe^{3+}.

$$CuFeS_{2(s)} + 4Fe^{3+} \rightarrow Cu^{2+} + 5Fe^{2+} + 2S^0 \quad (1)$$

Equation (1) can be considered to be the sum of anodic and cathodic half-cell reactions as shown in Equations (2) and (3) [12–15].

$$\text{Anodic half-cell reaction: } CuFeS_{2(s)} \rightarrow Cu^{2+} + Fe^{2+} + 2S^0_{(s)} + 4e^- \quad (2)$$

$$\text{Cathodic half-cell reaction: } 4Fe^{3+} + 4e^- \rightarrow 4Fe^{2+} \quad (3)$$

Chalcopyrite is frequently associated with pyrite (FeS_2), the predominant contributor to the serious environmental issue of acid and metalliferous drainage (AMD). However, to date the role of chalcopyrite in AMD is not well understood. In the absence of pyrite, both anodic and cathodic reactions occur on the chalcopyrite surface. The slow dissolution rate has been proposed to be due to a slow cathodic half-cell reaction on the chalcopyrite surface [11,16]. In the presence of pyrite, the cathodic half-cell reaction occurs on the pyrite surface as the rest potential of pyrite is greater (660 mV SHE) than that of chalcopyrite (560 mV SHE), forming a galvanic cell with electron transfer from the lower rest potential material (anode) to the material with the greater rest potential (cathode) material [3]. It has been reported that when chalcopyrite is in intimate contact with pyrite, the dissolution rate of chalcopyrite is increased significantly as compared chalcopyrite in isolation [11,14,17,18]. On the other hand, the dissolution rate of chalcopyrite is significantly decreased in the presence of sulfide minerals with lower rest potential such as sphalerite and galena [10].

Li *et al.* [19] have investigated the effect of E_h on chalcopyrite dissolution and found that the chalcopyrite dissolution rate at 750 mV is significantly greater than that at 650 mV. Further study has shown that the chacopyrite dissolution rate at 650 mV is increased in the presence of added soluble iron [20]. However, the effect of pyrite at these two E_h conditions (*i.e.*, 650 and 750 mV SHE) is not yet well understood. Hence, better understanding of chalcopyrite dissolution behaviour, in the presence of pyrite as a function E_h is of geochemical and industrial importance for minimising AMD and optimising Cu extraction during hydrometallurgical processing, respectively [21–23].

2. Experimental Section

2.1. Mineral Characterisation

The chalcopyrite sample used in this study was from Sonora, Mexico. The pyrite originated from Huanzala, Peru and was purchased from Ward's Scientific. Quartz, added as an inert material in this study, originated from Bolivia, NSW, Australia and was purchased from Geo Discoveries (Gosford, NSW, Australia). A chunk of each mineral, *i.e.*, chalcopyrite, pyrite and quartz, was crushed and subsequently rod milled to obtain a size fraction of 38–75 μm via wet sieving. The resulting sample was then sonicated to remove clinging fines, and dried at 70 °C in an oven purged with N_2. These samples were then placed into a plastic tube which was sealed after being filled with N_2 gas to minimise surface oxidation by air. All the samples were stored in a freezer prior to use. BET analysis (University of South Australia, Adelaide, Australia) indicated a surface area of 0.24 ± 0.04 $m^2\ g^{-1}$ for chalcopyrite and 0.39 ± 0.04 $m^2\ g^{-1}$ for pyrite. As quartz was not dissolved in the dissolution experiment, the BET was not performed.

X-ray powder diffraction Rietveld analysis (University of South Australia, Adelaide, Australia) indicated that the chalcopyrite sample contained 92 wt. % chalcopyrite, 2 wt. % quartz, 1 wt. % pyrite, 1 wt. % sphalerite and another 4 wt. % amorphous (or unidentified) component(s). This is consistent with the ICP-AES measurement (Table 1) suggesting a stoichiometry of 95.9 wt. % $Cu_{0.96}Fe_{0.99}S_{2.00}$ [24]. A stoichiometry for the pyrite samples of 94.3 wt. % $Fe_{1.91}S_{2.00}$ was also indicated (Table 1). This is in agreement with Rietveld XRD analysis of the pyrite which indicated the only phase present to be pyrite with approximately 4 wt. % amorphous. SiO_2, was determined to be of more than 99 wt. % purity by XRD analysis.

Table 1. Elemental composition of chalcopyrite and pyrite samples.

Element (wt. %)	S	Cu	Fe	Si	Ca	Bi	Zn	Pb	As	Al	Co	K	Mg
Chalcopyrite	34.1	32.5	29.3	0.9	0.8	0.3	0.5	0.3	0.06	0.04	0.1	0.02	0.02
Pyrite	51.5	0.01	42.8	-	0.01	-	0.01	0.004	0.003	0.01	-	0.006	-

Note: "-" less than detection limit (Si, Mg 0.003 wt. %, Bi, Co 0.001 wt. %).

2.2. Dissolution Conditions

Glass vessels (1.2 L) and dissolution cells (PTFE, 60 mL) were used for the flow-through dissolution experiments. The 5-port lid of the glass vessel provided access to the dissolution liquor and was used to house a thermometer, Teflon impeller, high temperature E_h probe, hydrogen peroxide (H_2O_2) inlet and a reflux condenser. The four blade Teflon impeller was driven by a digitally controlled stirrer with a constant agitation speed of 500 rpm. Heating was provided by a thermostatically controlled silicone oil bath. In addition to the glass vessels, a peristaltic pump (20 rpm min^{-1}) was used to recycle the dissolution solution between each vessel and the PTFE cell (60 mL) through connecting tubes. The PTFE cells were hosted and heated in an adjacent oven to the oil bath. Both the reaction vessels and the PTFE cells were maintained at 75 °C.

A total 10 g of sample ($38 < x < 75$ μm) was placed into the bottom of the flow-through cell. For the reference experiment 4 g of chalcopyrite and 6 g of quartz were mixed uniformly. In another cell 4 g of

chalcopyrite and 6 g of pyrite were mixed uniformly to investigate chalcopyrite dissolution in the presence of pyrite. A solution flow rate of 8 L d^{-1} was used. The leach liquor was controlled to have E_h of either 650 or 750 mV (SHE) to within ±10 mV, using 7.5 wt. % H_2O_2 solution, and an auto titrator (EUTECH pH 200 series (Thermo Scientific, Singapore) with a Master Flex pump (John Morris Scientific, Chatswood, Australia). The leach solution pH was checked during sampling and maintained at pH 1.0 by addition of 5 M sulfuric acid.

In order to better understand the surface S species on the leached chalcopyrite polished chalcopyrite and pyrite samples (8 × 8 × 5 mm, using 600 then 1200 grit silicon carbide paper) were used. The presence of pyrite in the dissolved residue containing the mixture of pyrite and chalcopyrite would perturb the interpretation of S species upon chalcopyrite surface. The reference experiment used one chalcopyrite slab and the chalcopyrite-pyrite galvanic couples was examined using one chalcopyrite and one pyrite slab tied together using cable ties. In both cases these samples were leached in 750 mV leach liquor at 75 °C and pH 1.0. The leach system that was used is described in [25] and in both instances a stirring speed of 500 rpm was applied. It has been shown that approximately 30% Cu was leached from powdered (38–75 μm) chalcopyrite at 30 h upon being subjected to this degree of agitation. Hence, it is reasonable to suggest that surface species differences due to galvanic interaction would be apparent after 30 h.

2.3. Bulk and Surface Analyses

During the dissolution process, 10 mL of the reaction solution was sampled periodically and filtered using a 0.22 μm membrane. The liquor was analysed for soluble Fe, Cu and S analysis using inductively coupled plasma—atomic emission spectroscopy (ICP-AES) by Analytical Chemistry Sector at Rio Tinto Technology and Innovation in Bundoora, Australia. Experimental uncertainty of the ICP-AES measurements was estimated to be around 1%. The reaction solution in the glass vessel was replenished upon each sampling with a fresh 10 mL of lixiviant to maintain the original volume.

At the end of each experiment, a portion of the leached residue was rinsed three times using pH 1.0 perchloric acid to remove any surface adsorbed species from the lixiviant. These solids were immediately frozen using liquid N_2 to minimise post-dissolution oxidation. These frozen samples were subsequently used for surface-sensitive X-ray photoelectron spectroscopy (XPS) analysis. The remaining solids were washed with distilled water and dried in the oven at 35 °C for XRD and SEM analysis.

A SEM (Phillips XL30 field emission SEM, Adelaide Microscopy, Adelaide, Australia) equipped with energy dispersive spectrometers (EDS) was employed to record images, using both backscattered (BSE) and secondary electron (SE) modes, and elemental quantification. XRD measurements, on selected residues, were measured using a Bruker D4 ENDEAVOR (University of Adelaide, Adelaide, Australia) with Co Kα1 = 1.78897 Å at 35 kV and 40 mA. A computer program DIFFRA.EVA (Version 3.0.0.9) from Bruker in conjunction with the crystallography open database (REV 30738 2011.11.2) was applied to identify mineral phases while quantitative phase analysis of the XRD data was performed using the Rietveld method with the aid of DIFFRAC.SUIT TOPAS (Version 4.2, Bruker, Melbourne, Australia).

The XPS instrument used was a Kratos Axis Ultra instrument (University of South Australia, Adelaide, Australia). The X-ray source was a monochromatic aluminium cathode running at 225 W with

a characteristic energy of 1486.6 eV. Pass energies of 160 and 20 eV were used for survey and high-resolution scans, respectively. The charge neutraliser was utilised to compensate for surface static charging resulting from electron emission. The area of analysis (Iris aperture) was a 0.3 × 0.7 mm slot; the analysis depth was less than 15 nm. The analysis vacuum was 4×10^{-9} Torr. To minimise the sublimation of elemental sulfur (S^0), the samples were sample stage was cooled using liquid N_2 (150 K). Details of the XPS data analysis methodology are described in [24].

3. Results

3.1. Dissolution

Figure 1a indicates no significant difference in the extracted Cu concentrations in the presence of quartz or pyrite within 132 days, the duration of the experiment, when E_h was controlled at 750 mV. Within the initial 40 days, the Cu extracted at 750 mV increased in a manner similar to that at 650 mV in the presence of pyrite; approximately 6% of the Cu was extracted during this stage. Subsequently, the concentration of the Cu in the 750 mV leach liquor increased significantly, considerably more than that in the 650 mV leach liquor, regardless of the presence of quartz or pyrite. Approximately 45% of the Cu was released within 132 days when the E_h was 750 mV. In contrast, the Cu concentration increased slowly from 40 days (approximately 6%) within 132 days (approximately 12% Cu) for the dissolution at 650 mV in the presence of pyrite. When chalcopyrite was dissolved at 650 mV in the presence of quartz, less than 2.5% Cu was released within 132 days, indicating that the presence of pyrite resulted in a significantly increase in Cu dissolution rate at 650 mV, due most likely to the galvanic interaction between chalcopyrite and pyrite.

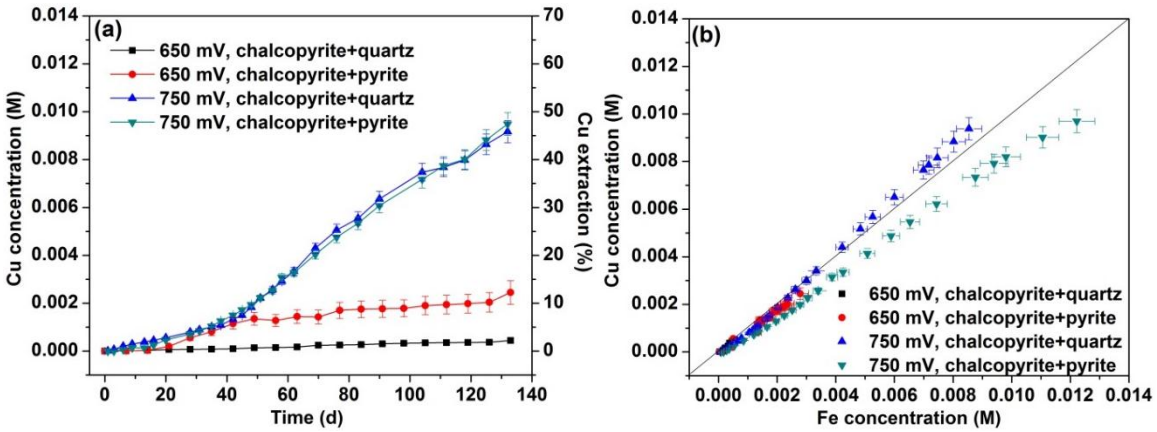

Figure 1. Leach data resulting from the flow-through experiments conducted at 75 ℃, pH 1.0, 650 mV and 750 mV: (**a**) Cu concentration and % extraction *versus* time; (**b**) Cu concentration against Fe concentration.

The Cu: Fe ratio was slightly greater than 1 when chalcopyrite was dissolved with quartz at 750 mV (Figure 1b). This ratio increased gradually, but was still close to 1, in the later dissolution stage when both Cu and Fe concentrations increased, indicating Cu to Fe stoichiometric dissolution of chalcopyrite. In contrast, when chalcopyrite was dissolved at 750 mV in the presence of pyrite, the Cu to Fe ratio was slightly less than 1 from the beginning of dissolution, and continued to decrease to approximately 0.8 at

the end of the experiment (*i.e.*, 132 days), indicating the dissolution of Fe from pyrite. However, the Cu to Fe ratio in the leach liquor was approximately 1 during the entire experiment duration when E_h was controlled at 650 mV, regardless of the presence of quartz or pyrite, indicating stoichiometric Cu–Fe dissolution of chalcopyrite.

3.2. XRD and SEM Analyses

Figure 2 shows the XRD patterns collected from the leach residues subjected to 750 mV, 75 ℃ and pH 1.0. Quantitative Rietveld analysis indicated a leach residue phase composition of 71 wt. % quartz, 19 wt. % chalcopyrite and 10 wt. % S^0 for the chalcopyrite-quartz leach system (Figure 2a) and 47 wt. % pyrite, 25 wt. % chalcopyrite and 28 wt. % S^0 for the chalcopyrite-pyrite system (Figure 2b). No other phases were identified. XRD patterns collected from the leach residues at 650 mV are not shown as most of the residues were almost identical to the feed (less than 12% of the chalcopyrite was dissolved, Figure 1a).

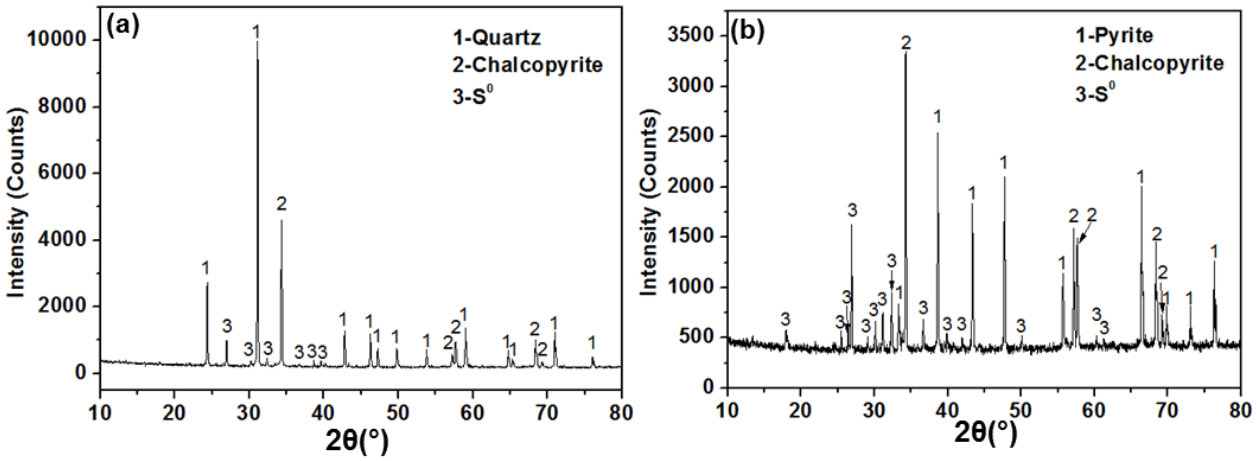

Figure 2. XRD patterns from the chalcopyrite leach residue subjected to 750 mV, 75 ℃ and pH 1.0: (**a**) chalcopyrite and quartz; (**b**) chalcopyrite and pyrite.

If the quantity of quartz (6 g) in the residues from the chalcopyrite-quartz system is assumed to be unchanged 1.607 g chalcopyrite and 0.845 g of S^0 are calculated to be present in the leach residue (Table 2). This weight of S^0 converts into 2.423 g of leached chalcopyrite. Hence, the total weight of chalcopyrite (remaining and dissolved) was 4.03 g which is nearly identical to that added initially (4 g). This suggests that approximately all of the sulfur from the chalcopyrite was oxidised to S^0, or alternatiely that no SO_4^{2-} was produced during chalcopyrite dissolution controlled at 750 mV, pH 1.0 and 75 ℃ (in the presence of inert quartz).

Table 2. Initial and final weights of mineral phases for the flow-through leach experiments. It is assumed that no quartz dissolution occurs.

	Remaining (Dissolved) Quartz	Remaining (Dissolved) Chalcopyrite	Remaining (Dissolved) Pyrite	S^0 Formed
4 g chalcopyrite + 6 g quartz	6 (0) g	1.607 (2.423) g	N.A.	0.845 g
4 g chalcopyrite + 6 g pyrite	N.A.	1.607 (2.423) g	3.021 (2.979) g	1.800 g

As shown in Figure 1a, Cu was dissolved in a similar manner in the presence of either quartz or pyrite at 750 mV, indicating an identical (within experimental error) quantity of chalcopyrite remaining in these two residues, *i.e.*, 1.607 g (equating to 25 wt. % of the leach residue in the presence of pyrite). Hence, the remaining total residue, and the amounts of pyrite and S^0 formed are calculated to be 6.428 g, 3.021 g and 1.800 g, respectively. If it is assumed that the leached chalcopyrite (*i.e.*, 2.423 g) produces 0.845 g of S^0 in the chalcopyrite-pyrite system, 0.955 g of S^0 must result from pyrite oxidation. This suggests that approximately 60% S (corresponding to 1.791 g of pyrite) of the leached pyrite (2.979 g) was oxidised to S^0 while 40% S (corresponding to 1.188 g of pyrite) from the pyrite was oxidised to soluble sulfur species, e.g., SO_4^{2-}.

Figure 3 shows SEM images, using two imaging modes, SE and BSE (e.g., Figure 3a,b) of the leach residues collected at 750 mV, 75 ℃ and pH 1.0. As indicated in Figure 3b, a portion of the chalcopyrite particles in the chalcopyrite-quartz leach system were oxidised to S^0, with the chalcopyrite particles being surrounded/armoured by S^0 (Figure 3c). In addition some chalcopyrite particles appeared unoxidised, presenting a smooth surface (Figure 3a,b).

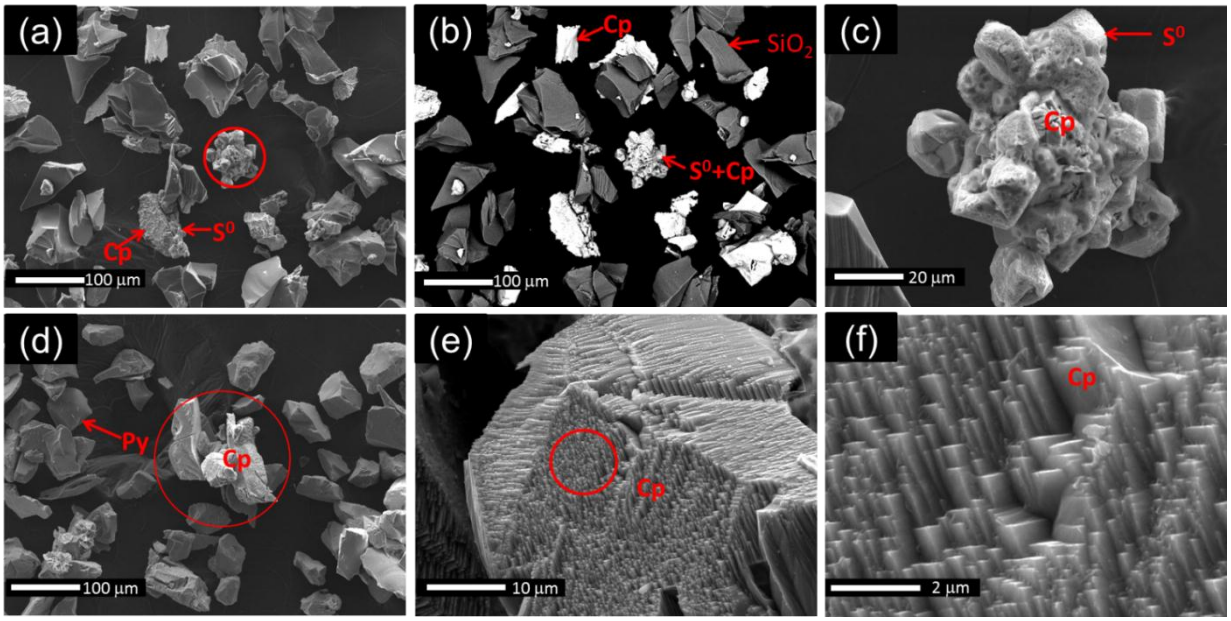

Figure 3. SEM images of leach residues collected at the end of the experiment, 132 days, (750 mV, 75 ℃ and pH 1.0 shown in Figure 1): (**a**) full view of chalcopyrite dissolved with quartz (SE image); (**b**) full view of chalcopyrite dissolved with quartz (BSE image); (**c**) selected area from (**a**); (**d**) full view of chalcopyrite dissolved with pyrite (SE image); (**e**) selected area from (**d**); (**f**) selected area from (**e**). Cp—chalcopyrite, S^0—elemental sulfur, SiO_2—quartz, Py—pyrite.

In contrast, when pyrite was present, the morphology of the oxidised chalcopyrite was significantly changed from that with in the chalcopyrite-quartz system. Figure 3d shows that both chalcopyrite and pyrite were present in the residue and Figure 3e indicates that the chalcopyrite surface was S^0-free. In addition, Figure 3e,f suggest that chalcopyrite dissolution behaviour may be different on different crystal faces. However, the interpretation of these images in terms of leach behaviour is not yet clear and will form a next step in our study.

3.3. XPS Analyses

XPS has been employed in order to understand the evolution of the uppermost surface species. As the presence of pyrite in the dissolved residue may convolute the interpretation of XPS S 2p species on the chalcopyrite surface, chalcopyrite slab surfaces leached in the glass vessel (instead of particles in the flow-through cell) were used.

Figure 4a shows that a significant amount of S^0 and S_n^{2-} (polysulfide) formed on the leached chalcopyrite surface in galvanic interaction with pyrite, as compared to that leached in isolation (Figure 4b). Figure 4c provides the difference spectra of Figure 4a minus Figure 4b. Figure 4d provides the fitting of the S 2p spectrum shown in Figure 4a. The presence of SO_4^{2-} on the chalcopyrite surface leached in isolation (Figure 4b) might be due to the slow leach rate. As water was used as the lubricating agent during the polishing process, the chalcopyrite surface may react with water to form SO_4^{2-}. But when chalcopyrite was contacting with pyrite, the increased leach would be expected to result in complete dissolution of SO_4^{2-} (Figure 4a).

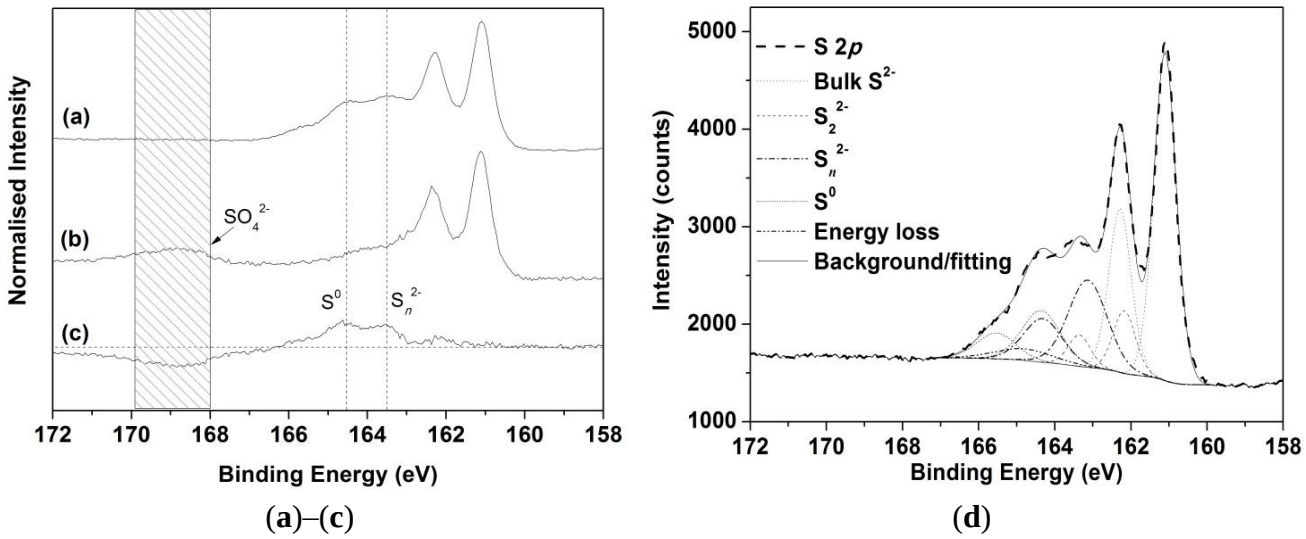

Figure 4. S 2p spectra collected from the chalcopyrite slabs dissolved at 750 mV, 75 ℃ and pH 1.0 for 30 h: (**a**) chalcopyrite from galvanic cell; (**b**) chalcopyrite only; (**c**) (**a**) minus (**b**); (**d**) fitting of (**a**).

Table 3 provides the quantification of S species on the surfaces of the chalcopyrite slabs. Both S_n^{2-} and S^0 are present in relatively greater quantities (as % of total S) where pyrite was in contact with the chalcopyrite as compared to the chalcopyrite only system, indicating enhanced sulfur oxidation occurred on the chalcopyrite slab surface involved in the galvanic cell.

However, these observations are apparently inconsistent with the dissolution data provided in Figure 1a which shows no enhancement in the Cu extraction rate in the galvanic chalcopyrite-pyrite system at 750 mV. In the flow-through dissolution experiment considerably greater Fe^{2+} is released from the chalcoyrite powder particles, as compared to the system used to leach the slab samples. This will be rapidly oxidised to Fe^{3+} which will dominate the subsequent dissolution (Equation (1)) at 750 mV. It is also worth considering that the absolute amount of surface S is not known. Hence although the relative amounts of oxidised S species (as % S) are greater on the chalcopyrite surfaces in contract with pyrite

(Table 3), the total S on these surfaces may actually be smaller as compared to those in contact with quartz. If this is the case so the absolute concentrations of the oxidised S species may also be smaller.

Table 3. S species (% S) on the leached chalcopyrite slab surfaces (30 h).

S Species	Binding Energy (eV)	FWHM * (eV)	Chalcopyrite Only	Chalcopyrite (Galvanic Cell)
Surface S^{2-}	160.6–160.8	0.5–0.6	3	0
Bulk S^{2-}	161.1	0.5–0.6	51	49
S_2^{2-}	161.8–162.2	0.6–0.7	5	7
S_n^{2-}	162.8–163.4	1.2–1.5	22	28
S^0	163.9–164.3	1.2–1.5	2	13
SO_4^{2-}	168.7–169.1	1.2–1.5	14	0
Energy loss	164.8–165.2	1.8–2.0	3	3

***** FWHM—full width at half maximum. For the estimation of FWHM values refer to [24,26].

No significant difference was observed between the O 1s spectra collected from chalcopyrite slab surface with and without pyrite present. Only chemisorbed H_2O and electrical isolated H_2O were observed in the O 1s spectra collected at these two surfaces, with no O^{2-} or OH^-/SO observed (Figure 5).

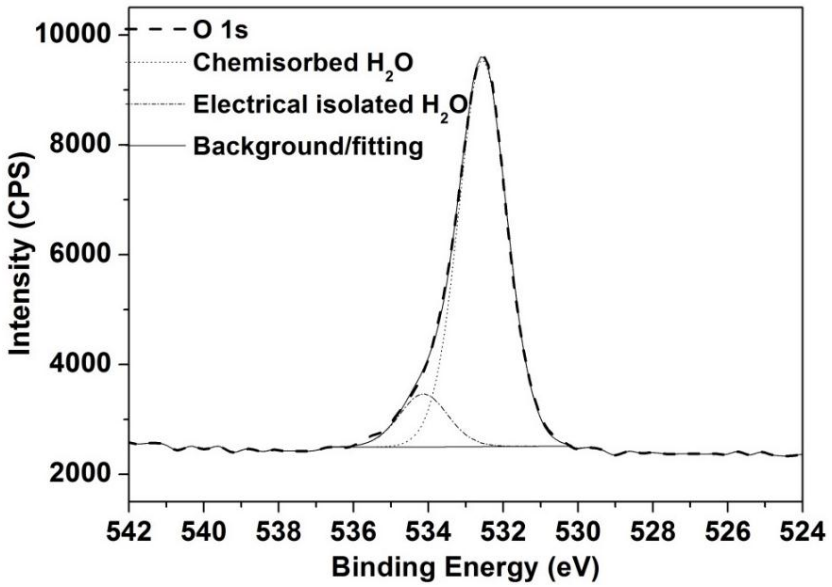

Figure 5. Fitted O 1s spectrum collected from the chalcopyrite slab in contact with pyrite (galvanic cell) leached at 750 mV, 75 ℃ and pH 1.0 for 30 h.

The strongest peak in the Fe $2p_{3/2}$ XPS spectra is observed at around 708 eV and another weak peak was also observed at 710–712 eV. This indicates that Fe(III)–S was the major Fe containing species with a component of Fe–O/OH also present [3,26–31] (Figure 6a). The Cu 2p spectrum (Figure 6b) shows that the oxidation stat of Cu in/on chalcopyrite was +1 [32–35].

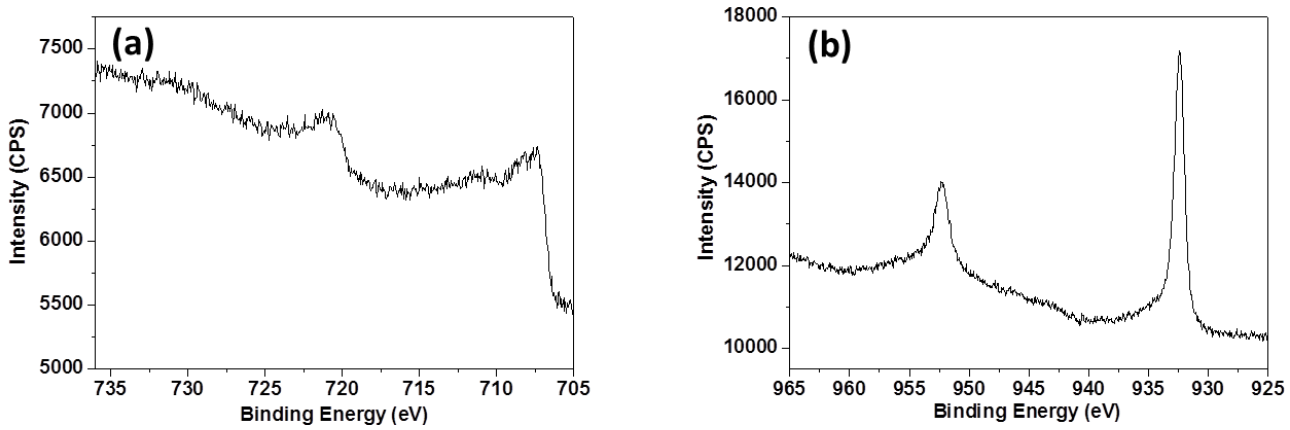

Figure 6. XPS spectra collected from the chalcopyrite surface in contact with pyrite (galvanic cell) leached for 30 h at 750 mV, 75 ℃ and pH 1.0: (**a**) Fe 2p; (**b**) Cu 2p.

4. Discussion

Equation (1) indicates that chalcopyrite can be oxidised by Fe^{3+} to produce S^0. As indicated by the Pourbaix diagram of the $CuFeS_2$–H_2O system [36], pH less than 4 and E_h greater than 580 mV (SHE) is required for effective Cu extraction from chalcopyrite. A greater Cu dissolution rate was observed at greater E_h (750 *cf.* 650 mV, Figure 1a), in accord with our previous chalcopyrite batch dissolution study [19].

The total Cu extracted from chalcopyrite at 650 mV increased significantly across the 132 days experimental duration when pyrite, as compared to quartz, was present (Figure 1a, 12% *cf.* 2.5%). Based on the ICP results (Figure 1a), the average Cu dissolution rate across 132 days at 650 mV is calculated to be 3.36×10^{-6} M d^{-1} in the absence of pyrite and 1.86×10^{-5} M d^{-1} when pyrite is present, indicating a fivefold increase of the Cu dissolution rate due to galvanic interaction. The mean chalcopyrite dissolution rate across 132 days at 750 mV is approximately four times greater than that at 650 mV in the presence of pyrite, *i.e.*, 7.11×10^{-5} M d^{-1} and 7.35×10^{-5} M d^{-1} for the chalcopyrite-quartz and chalcopyrite-pyrite systems respectively. This suggests that E_h plays a vital role in chalcopyrite dissolution rate-control. The similar Cu dissolution rates at 750 mV, in the presence and absence of pyrite, indicate that the galvanic interaction between chalcopyrite and pyrite is negligible.

Our findings are consistent with those of Tshilombo [37] who, using electrochemical techniques, reported that pyrite did not dissolve significantly at low solution potentials and under these conditions the leach rate of chalcopyrite was enhanced due to the presence of the cathodic sites on pyrite, *i.e.*, increased cathodic surface area. However, at greater solution potentials the galvanic interaction stopped and pyrite oxidation was apparent at redox potentials above 700 mV (SHE) [37].When Fe^{2+} is released from chalcopyrite or pyrite particles into solution, Fe^{3+} is available as the E_h is controlled and a portion of Fe^{2+} is oxidised rapidly by the addition of H_2O_2. The reduction of Fe^{3+} occurs on the pyrite surface in preference to the chalcopyrite surface when pyrite is present and contacting with chalcopyrite. However, when the solution E_h (e.g., 750 mV) is greater than the rest potential of pyrite, the reduction of Fe^{3+} on both pyrite and chalcopyrite is possible, resulting in the dissolution from both chalcopyrite and pyrite as indicated by Figure 1b. Therefore at 750 mV leaching of both chalcopyrite and pyrite is likely to take place. The dissolution of pyrite therefore increases the Fe concentration, resulting in a decreased Cu to

Fe ratio as shown in Figure 1b. However, stoichiometric Cu to Fe dissolution of chalcopyrite at 650 mV is expected (Figure 1b), regardless of the presence of pyrite, as this E_h is less than the rest potential of pyrite but greater than that of chalcopyrite [38] and little dissolution of pyrite occurs.

These findings are of significance in providing better understanding of the factors affecting dissolution rate of mixed chalcopyrite and pyrite systems in AMD systems within the most often observed E_h range of 500–800 mV (SHE) [39–41]. In particular the findings suggest that metalliferous Cu-containing drainage may be of importance in this E_h range and that acidic drainage from pyrite dissolution may be partially inhibited if the E_h remains below pyrite's rest potential. In addition, this study also reveals that the galvanic effect between chalcopyrite and pyrite (or other sulfides) in the hydrometallurgical processing of chalcopyrite can be managed via controlling the solution E_h.

5. Conclusions

Chalcopyrite leaching has been conducted at 75 ℃ and pH 1.0. At E_h of 650 mV, the presence of pyrite, as compared to the same amount of the inert mineral of quartz, increases chalcopyrite dissolution rate by more than five times due to the effective galvanic interaction between chalcopyrite and pyrite. In addition, chalcopyrite leaching of Cu and Fe was found to be stoichiometric suggesting insignificant pyrite dissolution.

The dissolution rate at 650 mV is significantly less than that at 750 mV, regardless of the presence of pyrite or quartz. At 750 mV the galvanic effect derived from pyrite is negligible as this E_h is greater than the rest potentials of both chalcopyrite and pyrite so that both minerals dissolve.

XRD and SEM results indicate that almost 100% S of the dissolved chalcopyrite is oxidised to S^0, regardless of the presence of pyrite (at 750 mV). When pyrite contacts with chalcopyrite at 750 mV, around 60% of the S due to pyrite leaching is oxidised to S^0 and the remaining 40% is released as soluble species, e.g., SO_4^{2-}. Therefore, a reasonable E_h should be selected if galvanic interaction is expected in chalcopyrite dissolution.

Acknowledgments

Financial support from Rio Tinto and Australian Research Council via the ARC-Linkage Project "Solution and surface speciation evolution during chalcopyrite leaching" (LP110200326) is gratefully acknowledged.

Author Contributions

Yubiao Li and Andrea Gerson wrote the paper and contributed to all the activities related to this paper. Gujie Qian cooperated in conducting the dissolution experiment and data analysis. Jun Li designed the dissolution experiment and contributed to all the discussion.

Conflicts of Interest

The authors declare no conflict of interest.

References

1. Córdoba, E.M.; Muñoz, J.A.; Blázquez, M.L.; González, F.; Ballester, A. Leaching of chalcopyrite with ferric ion. Part I: General aspects. *Hydrometallurgy* **2008**, *93*, 81–87.
2. Córdoba, E.M.; Muñoz, J.A.; Blázquez, M.L.; González, F.; Ballester, A. Leaching of chalcopyrite with ferric ion. Part III: Effect of redox potential on the silver-catalyzed process. *Hydrometallurgy* **2008**, *93*, 97–105.
3. Li, Y.; Kawashima, N.; Li, J.; Chandra, A.P.; Gerson, A.R. A review of the structure, and fundamental mechanisms and kinetics of the leaching of chalcopyrite. *Adv. Colloid Interface Sci.* **2013**, *197–198*, 1–32.
4. Watling, H.R. Chalcopyrite hydrometallurgy at atmospheric pressure: 1. Review of acidic sulfate, sulfate-chloride and sulfate-nitrate process options. *Hydrometallurgy* **2013**, *140*, 163–180.
5. Munoz-Castillo, B.P. Reaction Mechanisms in the Acid Ferric-Sulfate Leaching of Chalcopyrite. Ph.D. Thesis, University of Utah, Salt Lake City, UT, USA, 1977.
6. Hirato, T.; Majima, H.; Awakura, Y. The leaching of chalcopyrite with ferric sulfate. *Metall. Mater. Trans. B* **1987**, *18*, 489–496.
7. Klauber, C. A critical review of the surface chemistry of acidic ferric sulphate dissolution of chalcopyrite with regards to hindered dissolution. *Int. J. Miner. Process.* **2008**, *86*, 1–17.
8. Watling, H.R. The bioleaching of sulphide minerals with emphasis on copper sulphides—A review. *Hydrometallurgy* **2006**, *84*, 81–108.
9. Hiroyoshi, N.; Miki, H.; Hirajima, T.; Tsunekawa, M. Enhancement of chalcopyrite leaching by ferrous ions in acidic ferric sulfate solutions. *Hydrometallurgy* **2001**, *60*, 185–197.
10. Dutrizac, J.E. Elemental sulphur formation during the ferric sulphate leaching of chalcopyrite. *Can. Metall. Quart.* **1989**, *28*, 337–344.
11. Dixon, D.G.; Mayne, D.D.; Baxter, K.G. Galvanox (TM)—A novel galvanically-assisted atmospheric leaching technology for copper concentrates. *Can. Metall. Quart.* **2008**, *47*, 327–336.
12. Liu, Q.; Li, H.; Zhou, L. Galvanic interactions between metal sulfide minerals in a flowing system: Implications for mines environmental restoration. *Appl. Geochem.* **2008**, *23*, 2316–2323.
13. Koleini, S.M.J.; Jafarian, M.; Abdollahy, M.; Aghazadeh, V. Galvanic leaching of chalcopyrite in atmospheric pressure and sulfate media: Kinetic and surface studies. *Ind. Eng. Chem. Res.* **2010**, *49*, 5997–6002.
14. Koleini, S.M.J.; Aghazadeh, V.; Sandström, A. Acidic sulphate leaching of chalcopyrite concentrates in presence of pyrite. *Miner. Eng.* **2011**, *24*, 381–386.
15. Misra, M.; Fuerstenau, M.C. Chalcopyrite leaching at moderate temperature and ambient pressure in the presence of nanosize silica. *Miner. Eng.* **2005**, *18*, 293–297.
16. Tshilombo, A.F.; Petersen, J.; Dixon, D.G. The influence of applied potentials and temperature on the electrochemical response of chalcopyrite during bacterial leaching. *Miner. Eng.* **2002**, *15*, 809–813.
17. Berry, V.K.; Murr, L.E.; Hiskey, J.B. Galvanic interaction between chalcopyrite and pyrite during bacterial leaching of low-grade waste. *Hydrometallurgy* **1978**, *3*, 309–326.

18. Mehta, A.P.; Murr, L.E. Kinetic study of sulfide leaching by galvanic interaction between chalcopyrite, pyrite, and sphalerite in the presence of T. ferrooxidans (30 °C) and a thermophilic microorganism (55 °C). *Biotechnol. Bioeng.* **1982**, *24*, 919–940.
19. Li, Y.; Qian, G.; Li, J.; Gerson, A. The rate controlling parameters in the hydrometallurgical leaching of chalcopyrite. In Proceedings of ALTA 2014 Nickel-Cobalt-Copper Sessions, Perth, Australia, 24–31 May 2014; pp. 399–410.
20. Li, Y.; Qian, G.; Li, J.; Gerson, A.R. Kinetics and roles of solution and surface species of chalcopyrite dissolution at 650 mV. *Geochim. Cosmochim. Acta* **2015**, *161*, 188–202.
21. Li, J.; Kawashima, N.; Kaplun, K.; Absolon, V.J.; Gerson, A.R. Chalcopyrite leaching: The rate controlling factors. *Geochim. Cosmochim. Acta* **2010**, *74*, 2881–2893.
22. Kaplun, K.; Li, J.; Kawashima, N.; Gerson, A.R. Cu and Fe chalcopyrite leach activation energies and the effect of added Fe^{3+}. *Geochim. Cosmochim. Acta* **2011**, *75*, 5865–5878.
23. Kimball, B.E.; Rimstidt, J.D.; Brantley, S.L. Chalcopyrite dissolution rate laws. *Appl. Geochem.* **2010**, *25*, 972–983.
24. Li, Y.; Chandra, A.P.; Gerson, A.R. Scanning photoelectron microscopy studies of freshly fractured chalcopyrite exposed to O_2 and H_2O. *Geochim. Cosmochim. Acta* **2014**, *133*, 372–386.
25. Qian, G.; Li, J.; Li, Y.; Gerson, A.R. Probing the effect of aqueous impurities on the leaching of chalcopyrite under controlled conditions. *Hydrometallurgy* **2014**, *149*, 195–209.
26. Acres, R.G.; Harmer, S.L.; Beattie, D.A. Synchrotron XPS, NEXAFS, and ToF-SIMS studies of solution exposed chalcopyrite and heterogeneous chalcopyrite with pyrite. *Miner. Eng.* **2010**, *23*, 928–936.
27. Buckley, A.N.; Woods, R. An X-ray photoelectron spectroscopic study of the oxidation of chalcopyrite. *Aust. J. Chem.* **1984**, *37*, 2403–2413.
28. Smart, R.S.C. Surface layers in base metal sulphide flotation. *Miner. Eng.* **1991**, *4*, 891–909.
29. Fairthorne, G.; Fornasiero, D.; Ralston, J. Effect of oxidation on the collectorless flotation of chalcopyrite. *Int. J. Miner. Process.* **1997**, *49*, 31–48.
30. Brion, D. Photoelectron spectroscopic study of the surface degradation of pyrite (FeS_2), chalcopyrite ($CuFeS_2$), sphalerite (ZnS), and galena (PbS) in air and water. *Appl. Surf. Sci.* **1980**, *5*, 133–152.
31. Acres, R.G.; Harmer, S.L.; Shui, H.W.; Chen, C.H.; Beattie, D.A. Synchrotron scanning photoemission microscopy of homogeneous and heterogeneous metal sulfide minerals. *J. Synchrotron Radiat.* **2011**, *18*, 649–657.
32. Yin, Q.; Kelsall, G.H.; Vaughan, D.J.; England, K.E.R. Atmospheric and electrochemical oxidation of the surface of chalcopyrite ($CuFeS_2$). *Geochim. Cosmochim. Acta* **1995**, *59*, 1091–1100.
33. Harmer, S.L.; Pratt, A.R.; Nesbitt, H.W.; Fleet, M.E. Reconstruction of fracture surfaces on bornite. *Can. Mineral.* **2005**, *43*, 1619–1630.
34. Pearce, C.I.; Pattrick, R.A.D.; Vaughan, D.J.; Henderson, C.M.B.; van der Laan, G. Copper oxidation state in chalcopyrite: Mixed Cu d^9 and d^{10} characteristics. *Geochim. Cosmochim. Acta* **2006**, *70*, 4635–4642.
35. Klauber, C.; Parker, A.; van Bronswijk, W.; Watling, H. Sulphur speciation of leached chalcopyrite surfaces as determined by X-ray photoelectron spectroscopy. *Int. J. Miner. Process.* **2001**, *62*, 65–94.

36. Garrels, R.M.; Christ, C.L. *Solutions, Minerals, and Equilibria*; Harper & Row: New York, NY, USA, 1965.
37. Tshilombo, A.F. Mechanism and Kinetics of Chalcopyrite Passivation and Depassivation during Ferric and Microbial Leaching. Ph.D. Thesis, University of Brithish Columbia, Vancouver, BC, Canada, December 2004.
38. Payant, R.; Rosenblum, F.; Nesset, J.E.; Finch, J.A. The self-heating of sulfides: Galvanic effects. *Miner. Eng.* **2012**, *26*, 57–63.
39. Costa, M.; Martins, M.; Jesus, C.; Duarte, J. Treatment of acid mine drainage by sulphate-reducing bacteria using low cost matrices. *Water Air Soil Pollut.* **2008**, *189*, 149–162.
40. Borkowski, A.; Parafiniuk, J.; Wolicka, D.; Kowalczyk, P. Geomicrobiology of acid mine drainage in the weathering zone of pyrite-bearing schists in the rudawy janowickie mountains (Poland). *Geol. Q.* **2013**, *57*, 601–612.
41. Azzali, E.; Marescotti, P.; Frau, F.; Dinelli, E.; Carbone, C.; Capitani, G.; Lucchetti, G. Mineralogical and chemical variations of ochreous precipitates from acid sulphate waters (asw) at the Roşia Montană gold mine (Romania). *Environ. Earth Sci.* **2014**, *72*, 3567–3584.